DsTau status report

The DsTau Collaboration

Abstract

We report on the status and prospects of the DsTau experiment at the CERN SPS, with a focus on the pilot run in 2018, and the developments of the analysis chain from the readout of emulsion films to the detection of short-lived particle decays.

CERN-SPSC-2019-013 / SPSC-SR-250
26/05/2019

Contents

1 Introduction

DsTau has been proposed at the CERN SPS to study tau-neutrino production aiming at providing important data for future ν_τ studies [1]. A precise measurement of the ν_τ cross section would enable a search for new physics effects in ν_τ CC interactions. It also has practical importance for the next generation experiments for neutrino oscillation studies and astrophysical ν_τ observations. The practical way of producing a ν_τ beam is by the sequential decay of D_s mesons produced in high-energy proton interactions. However, there is no experimental measurement of the D_s differential production cross section in fixed target experiments using proton beams, which leads to a large systematic uncertainty on the ν_τ flux estimation. The DsTau project aims to reduce the systematic uncertainty in the current ν_τ cross section measurement to 10% or below, by measuring the D_s differential production cross section (especially longitudinal dependence). For this purpose, emulsion detectors with spatial resolution of 50 nm will be used, allowing the detection of $D_s \to \tau \to X$ double kinks in a few mm range. During the physics run, 2.3×10^8 proton interactions will be collected in the tungsten target, and 1000 $D_s \to \tau$ decays are expected to be detected. In addition to the primary aim, analyzing 2.3×10^8 proton interactions in tungsten and $\sim3\times10^8$ proton interactions in plastic and emulsions, combined with the high yield of $\sim 10^5$ charmed decays produced as by-products, will enable the extraction of additional physical quantities such as constraints for forward production of charm hadrons from intrinsic charm [2], and interaction length of charmed hadrons.

The year 2018 was mainly devoted to the preparation, execution and post-processing of the pilot run. In parallel, we have constructed the analysis chain from the emulsion readout to the detection of short-lived particle decays. The flowchart of the chain is given in Figure 1. Here we present the progress in each part.

2 Summary of the 2018 pilot run

The aim of this run was to perform a 1/10 scale measurement and establish a full chain of analysis. With this run about 80 $D_s \to \tau \to X$ events are expected to be detected. We aim to obtain the first measurement of D_s differential production, which would already allow us to re-evaluate the DONuT ν_τ cross-section measurement by reducing the systematic uncertainty on the ν_τ flux from >50% to 30% level. The pilot run was performed from 22^{nd} to 29^{th} August. 10 people from 6 institutes joined the exposure campaign at the H2 beamline in the North Area.

A total of 50 m^2 of emulsion films were produced for DsTau, whose production was shared by two facilities in Bern and Nagoya. The DsTau collaboration organized shifts from May to August to distribute the workload. The emulsion films were shaped into 12.5 cm × 10 cm, yielding about 4,000 films, corresponding to 30 DsTau modules (131 films per module). The detector modules were assembled in the dark room at CERN.

The DsTau detector setup consisting of the target mover, silicon pixel telescope and scintillation counter was mounted on the movable table at the H2 beamline, as shown in Figure 2. The SPS experts helped to realize a large beam size of about 20 mm × 20 mm, as shown

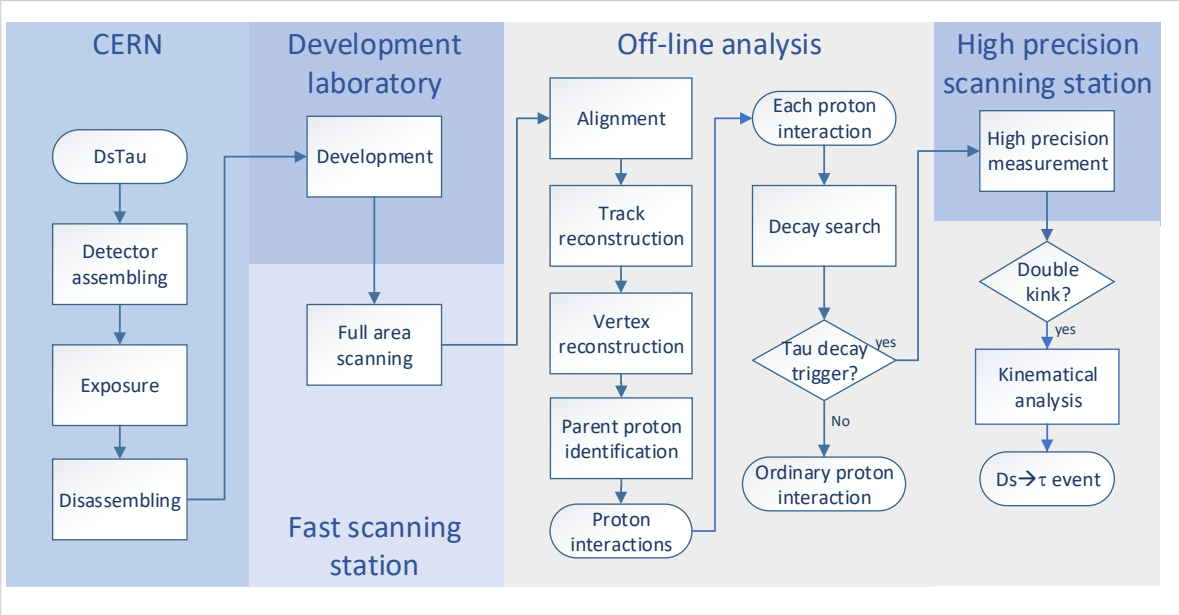

Figure 1: Flowchart from the emulsion readout to the $D_s \to \tau$ event detection.

in Figure 3 obtained by the silicon pixel telescope.

The emulsion detector modules were put on the target mover to scan with respect to the proton beam. The targeting beam density on the module surface was set to be 0.9–1.0$\times 10^5$ protons/cm^2. The exposure was performed with a beam intensity about 3×10^5 protons per spill. As the proton intensity in a flat-top varies in time, the actual beam intensity was monitored by the scintillation counter and fed back to the target mover control, so that a uniform irradiation to the module was performed. The time needed to expose a module strongly depended on the super-cycle structure of the SPS. If there is only one flat-top in a super-cycle with the LHC filling, it took more than 1 hour. While, if there are two flat-tops in a super-cycle, it took only 20 minutes. In addition, the exchange of the modules had an overhead of 10 minutes. With a stable beam, an average speed of 50 minutes per module was achieved including the overhead time (recorded on Saturday 25$^{\text{th}}$ August). The integrated protons collected by this run is shown in Figure 4. In total about 3.5$\times 10^8$ protons were collected in the 30 modules (the exposure team is shown in Figure 5).

The exposed films were disassembled at CERN and brought to the University of Bern, where the chemical processing was performed (Figure 6). The development of all 4000 films took about 3 weeks. The developed films were once sent to the collaborators to remove the so-called "surface silver". Then they were sent to Nagoya University for the fast readout. Just before reading out by the scanning microscope, the thickness of the emulsion layers was tuned to be the same as before development by adding glycerin in the emulsion layer.

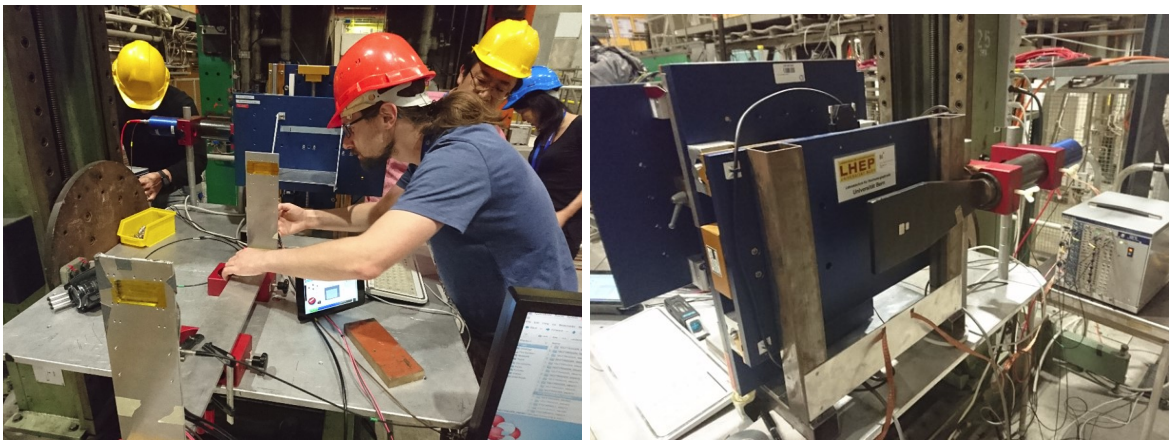

Figure 2: Installation of the setup.

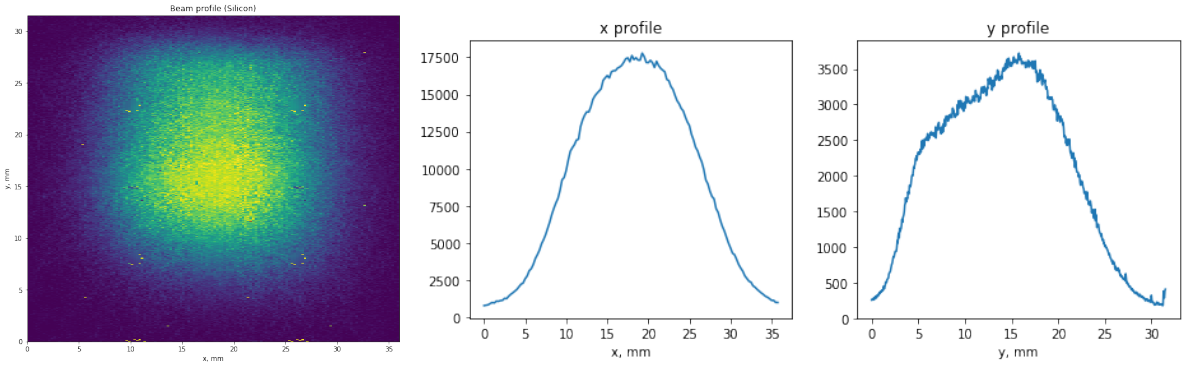

Figure 3: Measured profile by the silicon detector (by scanning). Left: Reconstructed profile in 2D (36 mm $\times$ 31.6 mm). Middle and Right: X and Y projections.

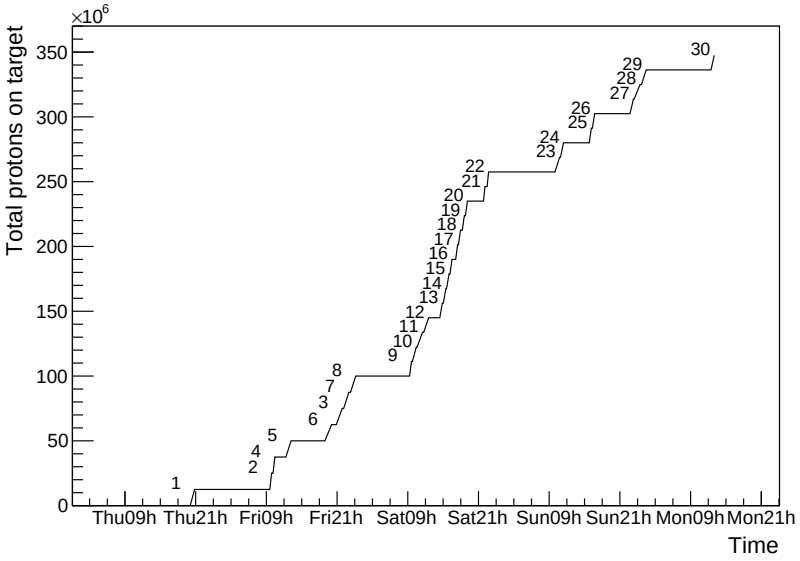

Figure 4: Integrated POT during the beam time. The number in the plot shows the id of the detector modules.

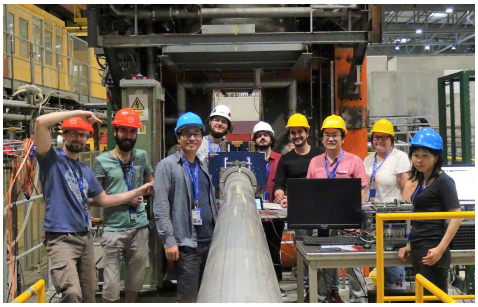

Figure 5: The exposure team after completion of the data taking.

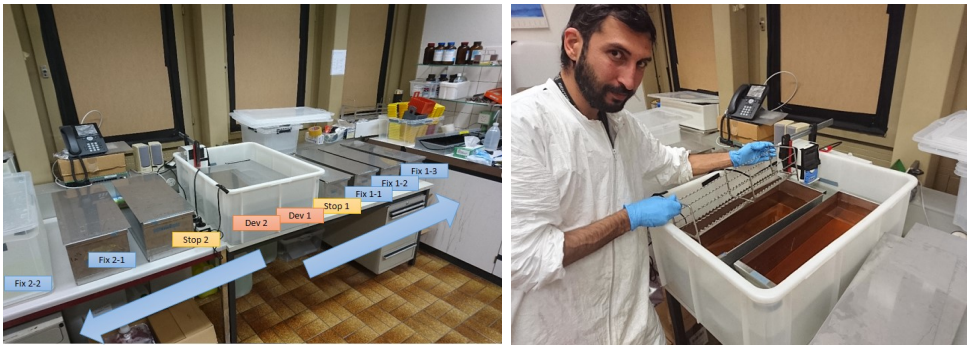

Figure 6: Photos of the development facility in the University of Bern.

3 Readout and data analysis

3.1 Readout of emulsion films

The emulsion detector is both a detector and the data storage media at the same time. In order to perform an efficient detection of the small kinks of $D_s \to \tau$ decays, the analysis is performed in two stages: (1) scan the full detector by a fast system HTS [3] with the standard angular resolution and detect events those have two decays in a short distance, namely the decays of τ and partner charm (D^0 or $D^{\pm}$). (2) perform a high precision measurement around the τ decay candidates to find $D_s \to \tau$ small kinks.

The scanning of the emulsion films from the pilot run was started in the beginning of November 2018. The progress of the scanning is shown in Figure 7 (right). The bare scanning time for an emulsion film (12.5 cm $\times$ 10 cm) is about 6 minutes. Currently the progress speed is limited by the machine time of the HTS and the film exchanging time. Figure 7 (left) shows the number of scanned films per day. It shows a boost in November and December by the shifters from the collaboration, performing night-shifts. From January 2019, the machine time for DsTau is 11 hours per week, yielding to 26 films/week. An optimization of work scheme is foreseen to increase this speed to 50 films/week. As shown in Table 1, 5.7 modules were scanned so far, corresponding to 19% of the films to be scanned in the pilot run. The fast readout of all the films is expected to be accomplished by the end of 2019.

The machine time of the HTS is currently shared by several experiments. By the time of the physics run in 2021/2022, an additional HTS (HTS II, a 5 times faster system) will be available. We will continue to use the current HTS, because the film exchanging time is anyway the significant part of the scanning for this project.

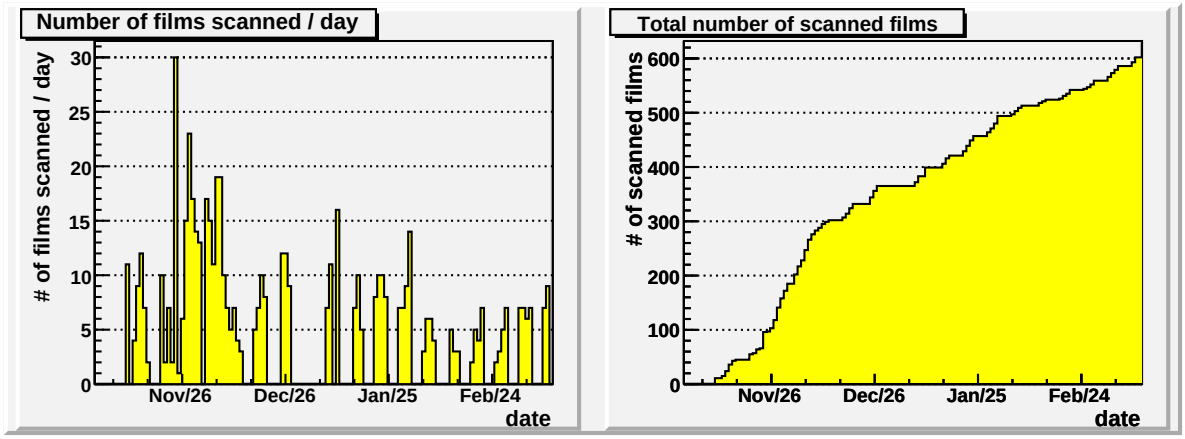

Figure 7: Number of scanned films per day (left) and the integrated number of scanned films (right). The mean speed is 26 films/week and the peak speed achieved so far is 30 films/day.

	Number of modules	Fraction to 30 modules
Surface silver removed	13	43.0%
Swelling performed	7	23.3%
Scanning performed	5.7	19.0%

Table 1: Status of emulsion readout.

3.2 Off-line analysis

The raw image data amounts about 20 TBytes/film. This is reduced by online processing of the HTS to 4-30 GBytes/film depending on track density, and stored in the disk. The stored information is the track segments recorded in the top and bottom layers of films (*microtracks*). By connecting the microtracks on both layers, *basetracks* are formed, which are a basic unit for latter processing. Each basetrack provides 3D coordinates $\vec{X} = (x, y, z)$, 3D vector $\vec{V} = (\tan\theta_x, \tan\theta_y, 1)$ and dE/dx parameters.

The basic concept of track reconstruction is to link basetracks on different films by using their position and angular correspondences. The track density in DsTau ($10^5 - 10^6/\mathrm{cm}^2$ in small angular space) is relatively high. The conventional reconstruction tools for OPERA, which had a track density of $10^2 - 10^3/\mathrm{cm}^2$ in large angular space, are often not appropriate. The conventional algorithm is based on a correspondence test between basetracks on two consecutive films. It has a difficulty in the reconstruction in high density environment like in DsTau. Especially if two or more tracks with similar track angles (in a few mrad) come close (in a few micron), the algorithm may not resolve the right paths.

A new tracking algorithm was developed to reconstruct tracks in the environment with high track density and narrow angular spread. When it faces multiple path candidates, it allows to keep all possible paths. For the case in Figure 8 (a), $2^4 = 16$ possible paths are considered between Z_1 to Z_2. For each path, a test variable based on topological area made by basetracks involved in the possible paths is evaluated,

$$a^{average} = \left(\sum_{i}^{n-2} a^{pos} + \sum_{i}^{n-1} a^{angle} \right) / (n - 0.5).$$

Here, $a^{average}$ is an averaged area made by basetrack positions, a^{pos}, and one by basetrack angle, a^{angle}, as shown in Figure 8 (b). n is the number of basetracks involved in the path and -0.5 is an empirical value to put a higher weight on longer paths. The path with the smallest a^{sum} is chosen to be the best one. This procedure is repeated by removing the basetracks involved in the chosen paths.

An example of the reconstructed data from the detector is shown in the Figure 9 (left), which shows about ten thousand tracks in 2 mm$\times$ 2 mm ($\simeq 2.5 \times 10^5/\mathrm{cm}^2$).

The basetrack efficiency is measured by using reconstructed tracks and shown in Figure 9 (right). The average beastrack efficiency is higher than 95%. Although it is a minor effect, there is a downward trend of the efficiency along the depth in the module. This is likely due to the increase of track density. The measured basetrack efficiency is high enough to assure the track detection with high efficiency (>99%).

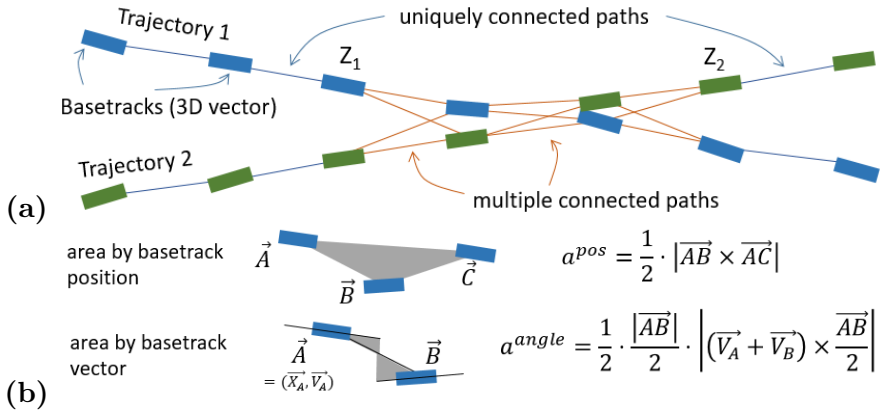

Figure 8: **(a)** Two tracks come closer and there are multiple possibilities in finding paths. **(b)** Areas made by basetracks, that are used to select the best possible paths.

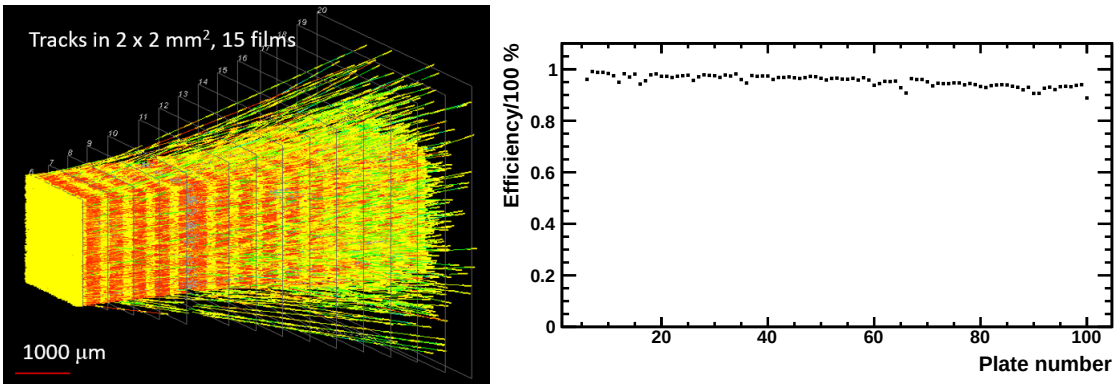

Figure 9: Left: 3D display of reconstructed tracks. Right: Basetrack efficiency film by film (2016 sample).

The data processing is divided into sub-volumes, for example 2 cm × 2 cm × 30 emulsion films. A preliminary alignment between each two consecutive films (transverse position shifts and gap) is obtained by means of penetrating tracks, which gives an alignment error of sub-micron in transverse direction. While, the propagation of error over tens of films is not negligible. To further improve the tracking resolution, an additional alignment procedure is applied by selecting 400-GeV proton tracks those are supposed to be most straight. The obtained alignment precision with 15 films as a function of data processing unit diameter is shown in Figure 10 (left). The algorithm assures a sub-micron alignment in relatively large reconstruction unit of 2 cm× 2 cm× 15-30 films. The alignment precision has a dependence on the processing area size, which is due to the distortion of plastic base.

In order to test the quality of the alignment and reconstruction, the proton beam tracks were studied in detail. The beam angular distributions measured in 2 cm × 2 cm × 15 films (7 mm thick) are shown in Figure 11 (left and middle). Approximated by Gaussian, the distribution has standard deviation of 110 µrad in XZ projection and 300 µrad in YZ. The

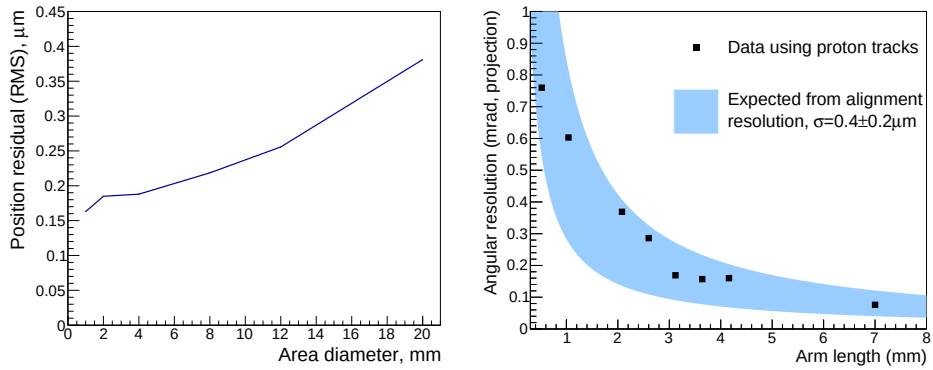

Figure 10: Left: Alignment resolution obtained in data as a function of the diameter of data processing unit. Position displacement of basetracks from the reconstructed track (a straight line) is evaluated. Right: Angular resolution of tracks as a function of reconstructed track length.

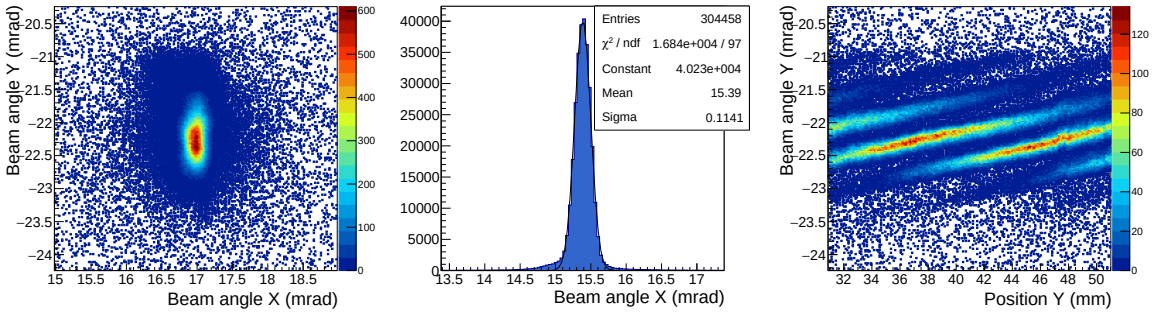

Figure 11: Left: Angular distribution of proton tracks. The angular range is ±2 mrad. Middle: X projection. The sigma of distribution is 110 µrad. Right: Beam angle Y as a function of Y coordinate. Each line corresponds to the exposure with a given Y coordinate. The positive correlation with position Y (slope of 0.44 mrad/cm) demonstrates the beam divergence.

width in angular distribution reflects the beam divergence of beam. The beam position profile was wider in YZ projection, therefore the beam divergence was also larger in YZ. Figure 11 (right) is the Y position dependence of beam angle in YZ, showing a strong pattern. Each inclined line in this plot corresponds to an exposure at a given Y position of the target mover. And the positive slope of the lines (440 µrad/cm) demonstrates that the beam is diverging. From the same plot, one can see that the track angular resolution is better than 100 µrad in the large volume. When one of the lines is fitted, the standard deviation of track slopes from the fit was found to be 76 µrad. The angular resolutions with reconstructed tracks as a function of track length is shown in Figure 10 (right).

The track density in the detector module rises with the depth in the detector. The measured number of tracks is compared with the FLUKA simulation as shown in Figure 12 (left). The track density at the beginning of decay module is about $1\times10^5/\mathrm{cm}^2$, and

increases to $5 \times 10^5/\mathrm{cm}^2$ in the last plates. The increase of track density is due to the proton interactions and also daughter hadron interaction and electromagnetic showers. Note that the total amount of material in the detector module corresponds to $0.1\lambda_{int}$ (0.05 by tungsten target, 0.05 by emulsion and plastic films), and $1.8X_0$ ($1.4X_0$ by tungsten). Although the track density increases, it has a minor effect on the reconstruction since the measurements in the emulsion detector are not just points in space but micro-vectors with precise position and direction. The reconstruction quality (mis-connections, etc) would degrade if too many tracks will coincide both in their position and angular space. However, the secondary tracks in the detector have a large variety of angles, and the track density in angular space is not in fact increasing, as shown in Figure 12 (right). The plot shows the relative angle of tracks with respect to the proton beam angle. While the tail of relatively large angles increases, the track density in the region close to the beam direction ($\theta = 0$) decreases because of proton interactions.

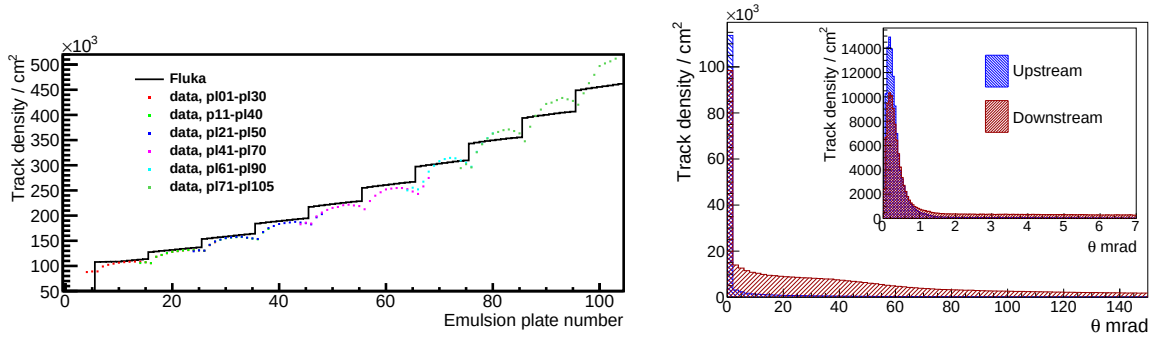

Figure 12: Left: The evolution of track density as a function of depth, compared with the FLUKA simulation. Right: Comparison of track angular density (tracks/cm^2/bin) between an upstream unit and downstream.

The reconstructed tracks are then used to find vertices. Using the tracks with the angle $\tan\theta <= 0.4$ rad, conversing pattern with 4 or more tracks are considered as a vertex. Once a vertex is found, the parental proton track which has a minimum distance to the vertex within 3 µm is searched for. If the parent proton track is found, the vertex is considered as a primary proton interaction. Figure 13 shows the reconstructed vertex Z distribution near by the tungsten target. An enhancement of vertices in the tungsten target is evident. One can even see the micro-structure corresponding to the emulsion layers (high density) and plastic bases/spacers. Figure 14 shows the measured multiplicity of charged particles at proton interactions, compared with the prediction by FLUKA. Further study will be performed on the products of proton interactions.

A systematic search for the decay topology of short-lived particles is applied for the found vertices. Events with short-lived decay topology are selected by requiring the following criteria.

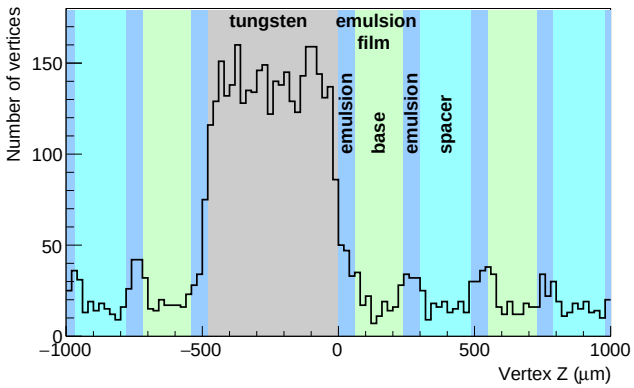

Figure 13: Reconstructed vertex position distribution in Z. The correspondence with the detector structure is clearly visible.

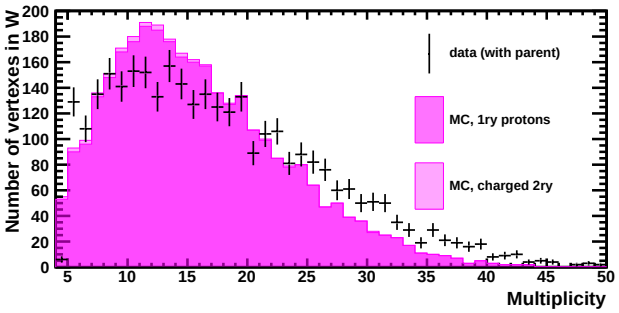

Figure 14: Measured multiplicity of charged particles at the proton interaction vertices compared with the prediction from FLUKA simulations.

For charged particle decays (1-prong, 3-prong):

- the parent is detected in at least two emulsion films
- the flight length of the parent is $\leq$ 10 mm
- the decay vertex is not in tungsten plates
- the angle of the parent tan$\theta \leq 0.3$
- the angle of the daughter tan$\theta \leq 0.5$
- the angle difference between the parent and the daughter is ≥ 0.01 rad and ≤ 0.5 rad
- the impact parameter of the daughter with respect to the primary vertex is ≥ 10 μm and ≤ 500 μm
- the daughter has to pass through the next tungsten plate and the angle difference before and after the plate is $\leq$ (0.003+0.025$\times$tanθ) rad

For neutral particle decays (2-prong):

- the parent passes through at least one emulsion film
- the flight length of the parent is $\leq$ 5 mm
- the decay vertex is not in tungsten plates
- the angle of the parent calculated from the positions of the primary and secondary vertices tan$\theta \leq 0.3$
- the angle of the daughter tan$\theta \leq 0.5$
- the angle difference between the parent and the daughter is ≤ 0.3 rad
- the impact parameter of the daughter with respect to the primary vertex is ≥ 10 μm and ≤ 300 μm
- the daughter has to pass through the next tungsten plate and the angle difference before and after the plate is $\leq$ (0.003+0.025$\times$tanθ) rad
- the opening angle of the daughters is ≥ 0.01 rad

The selected statistics in a subsample of data is shown in Table 2. The expected signal normalized to the analyzed data is also given.

	Subsample in 2016 run		Subsample in the pilot run	
Analyzed protons (normalization)	3712959		3355967	
	Data	Expected	Data	Expected
Vertices in tungsten	19008	18567.2	17001	16779.1
Double decay topology	10	9.1	10	8.2

Table 2: Statistics found in the sub-sample of data.

An example of double charm event is shown in Figure 15. The proton interaction vertex occurred in tungsten 0.25 mm from the first downstream emulsion film. There are 18 charged particles at the proton interaction vertex (v^{1ry}), conversing with a mean minimum distance to the vertex (impact parameter) of 1.6 µm. One of those has a kink at 3.32 mm from v^{1ry}. The impact parameter of kink daughter to v^{1ry} is 174 µm. Additionally, two charged particles start 2.20 mm downstream of v^{1ry} with an opening angle of 0.132 radian. The plane made of these two particles has 15.2 mrad tilted with respect to the possible neutral parent vector,

meaning that this neutral decay is not two body decay. Such an event proves that our analyses of short-lived particles in the actual experimental conditions are possible.

So far our main effort was devoted to the establishment of the algorithms and pipeline, which has been established and running. The current bottleneck is the processing speed in the alignment and decay search. We will implement both a parallel processing with GPUs (suited for alignment) and a distributed computing using computing clusters (for decay search). Once these implementation was done, the offline processing would quickly catch up with the scanning.

In 2019, we will complete the emulsion readout for the 2018 pilot run and establish a framework for the precision measurements to detect $D_s \to \tau$ small kinks.

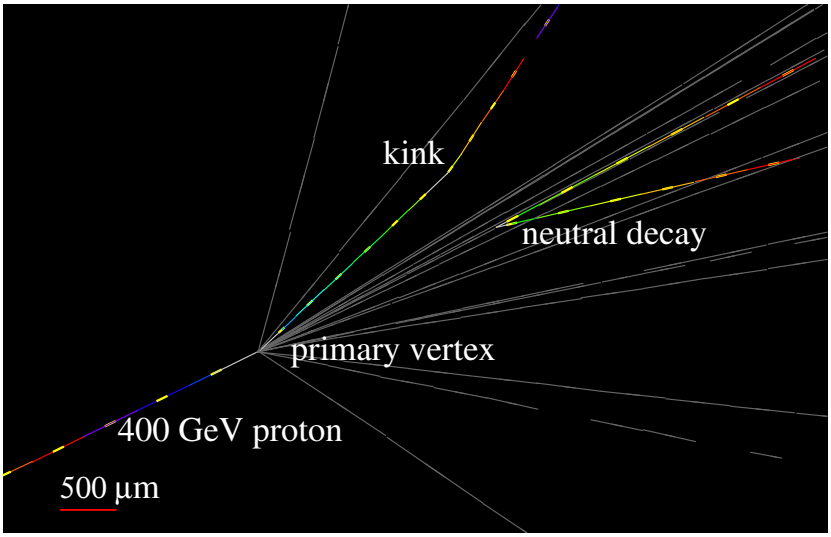

Figure 15: A double charm candidate event with a neutral 2-prong (vee) and a charged 1-prong (kink) topology. (tilted view)

4 Background study

The main background to $D_s \to \tau \to 1$ prong events are due to hadron interactions that mimics D_s decay. The probability of background event appearance is calculated as follows,

$$P_{\mathrm{BG}}^{D_s \to \tau \to 1 \text{ prong + pair charm}} = P_{\mathrm{int}} \cdot P_{\mathrm{BG}}^{D_s \to \tau} \cdot P_{\mathrm{BG}}^{\tau \to 1 \text{ prong}} \cdot P_{\mathrm{BG}}^{\text{pair charm}}.$$

Here, P_{int} is the probability of a primary proton to interact in the tungsten target in the decay module. $P_{\mathrm{BG}}^{D_s \to \tau}$, $P_{\mathrm{BG}}^{\tau \to 1 \text{ prong}}$ and $P_{\mathrm{BG}}^{\text{pair charm}}$ are the probabilities of secondary hadron interactions to be identified as $D_s \to \tau$, $\tau \to 1$ prong and pair charm decays, respectively.

These probabilities are obtained by simulating 3×10^5 protons on the detector with the FLUKA [4, 5] simulation tools. The criteria, used for charged charm or tau decay topology selection, are applied to interactions of secondary hadrons with only one charged daughter

particle ($P > 2$ GeV/c). Most of selected interactions have associated nuclear fragments, which is a strong evidence of hadron interactions.

The sources of background to neutral pair charm appearance are secondary neutral particle interactions and charged particle which interact within 2 emulsion plates downstream the charged particle origin, some of such short tracks are not reconstructed. These interactions can be associated with every primary proton interaction occurred upstream. To estimate the background probability to neutral charm topology, each neutral particle interaction and each charged particle, interaction withing 2 emulsion plates from it's origin, were selected and connected with every primary proton interaction vertex occurred upstream in tungsten. The selection criteria used for neutral pair charm search, described in the previous section, were applied to each primary-secondary interactions couple. Search for nuclear fragments associated with secondary interaction allows suppressing background in this channel as well.

The probability of primary proton interaction in tungsten and the probabilities of background event appearance with a certain path length and kink angles θ_{kink} and opening angle between daughters θ_{open} used for different signal channels are shown in Table 3. The total probabilities to register background events to double kink with charged pair charm or with neutral pair charm are $1.3 \pm 0.6 \times 10^{-9}$ and $2.7 \pm 0.8 \times 10^{-9}$, respectively. The expected numbers of background events in the full physics run statistics (4.6×10^9 p.o.t.) are 6.0 ± 1.8 and 12.4 ± 3.7 for these 2 signal channels, respectively.

Category	Criteria	Probability
$P_{\text{interaction}}$	interactions in the decay module	$(5.00 \pm 0.04) \times 10^{-2}$
$P_{\text{BG}}^{D_s \to \tau}$	2 mrad $< \theta_{\text{kink}} <$ 30 mrad 0.1 mm $<$ path length $<$ 5 mm	$(0.97 \pm 0.25) \times 10^{-3}$
$P_{\text{BG}}^{\tau \to 1 \text{ prong}}$, $P_{\text{BG}}^{\text{charged charm}}$	20 mrad $< \theta_{\text{kink}} <$ 500 mrad 0.1 mm $<$ path length $<$ 5 mm	$(5.1 \pm 0.6) \times 10^{-3}$
$P_{\text{BG}}^{\text{neutral charm}}$	$\theta_{\text{open}} >$ 10 mrad 0.1 mm $<$ path length $<$ 5 mm	$(10.9 \pm 0.9) \times 10^{-3}$
$P_{\text{BG}}^{D_s \to \tau \to 1 \text{ prong + charged charm}}$	$P_{\text{int.}} \cdot P_{\text{BG}}^{D_s \to \tau} \cdot P_{\text{BG}}^{\tau \to 1 \text{ prong}} \cdot P_{\text{BG}}^{\text{charged charm}}$	$(1.3 \pm 0.4) \times 10^{-9}$
$P_{\text{BG}}^{D_s \to \tau \to 1 \text{ prong + neutral charm}}$	$P_{\text{int.}} \cdot P_{\text{BG}}^{D_s \to \tau} \cdot P_{\text{BG}}^{\tau \to 1 \text{ prong}} \cdot P_{\text{BG}}^{\text{neutral charm}}$	$(2.7 \pm 0.8) \times 10^{-9}$

Table 3: Probability of hadron interactions mimicking the specific decay topology.

5 Plan for the physics run

During the physics run(s) beyond the LS2, we plan to expose 340 modules to the proton beam to collect 2.3×10^8 proton interactions in the tungsten target and to detect 1000 $D_s \to \tau$ decays (including the 30 modules from the pilot run to the data sample). Considering the limitation from the emulsion gel and film production, we would split the physics run into two runs in 2021 and 2022. We plan to expose 150 modules in the 2021 run. The achieved exposure speed in the pilot run was 50 minutes per module. Taking into account an effective data taking of 16 hours per day (including accelerator efficiency), we expect 19.2 modules to be exposed per day. Therefore the exposure of 150 modules will fit within two weeks of beam time, including the installation and dismantling of the setup. We would plan to expose the remaining 190

modules in 2022. The expected precision of the measurement as a function of the number of detected events is shown in Figure 16.

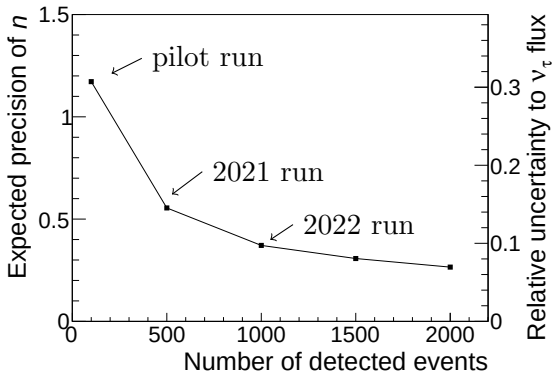

Figure 16: Expected precision for the measurement of parameter n as a function of the number of detected $D_s \to \tau \to X$ events. The estimated relative uncertainty of the ν_τ flux is also given as the y-axis on the right (a la DONUT).

The total cost for emulsion films for the physics runs is estimated to be 380 kCHF (the increase of cost with respect to the proposal is due to the change of emulsion layer thickness). About 30% of the required funding for emulsion films has already been allocated by the Kyushu and Nagoya groups. The DsTau Collaboration will keep trying to secure the remaining funding. An approved status of the project would certainly be of help to acquire funds by giving long-term perspective.

Taking into account that the film exchanging time is one of the limiting factors of the readout speed, an optimization of emulsion film size is under discussion. By employing twice larger film, the film exchanging time would be reduced to half. This modification will not affect the physics performance nor the cost for emulsion films.

6 Summary and outlook

The 2018 pilot run was successfully conducted. The analysis chain from the readout of emulsion films to the detection of short-lived decay topology has been established and is being applied to the analysis of the pilot run data. First physics results on $D_s \to \tau$ measurements and forward production of charm hadrons are foreseen within a year.

The physics run is planned in 2021 and 2022. We will expose total 340 modules and aim to conduct the readout and analysis within two years by increasing the machine time of the fast scanning system for DsTau and improving the off-line analysis speed.

References

[1] S. Aoki et al. [DsTau collaboration], CERN-SPSC-2017-029, SPSC-P-354 (2017), https://cds.cern.ch/record/2281295?ln=ja#.

[2] Weidong Bai and Mary Hall Reno, Prompt neutrinos and intrinsic charm at SHiP, JHEP02(2019)077.

[3] M. Yoshimoto, T. Nakano, R. Komatani and H. Kawahara, PTEP 10 (2017) 103.

[4] T. T. Böhlen., F. Cerutti, M. P. W. Chin, A. Fasso, A. Ferrari, P. G. Ortega, A. Mairani, P. R. Sala, G. Smirnov and V. Vlachoudis, The FLUKA Code: Developments and Challenges for High Energy and Medical Applications, Nucl. Data Sheets **120** (2014) 211.

[5] A. Ferrari, P. R. Sala, A. Fasso and J. Ranft, FLUKA: A multi-particle transport code, CERN-2005-010, SLAC-R-773, INFN-TC-05-11.